Thermal Stability of Endohedral First-Row Transition-Metal TM@Zn$_i$S$_i$ Structures, i = 12, 16

Elisa Jimenez-Izal*, Jon M. Matxain, Mario Piris, Jesus M. Ugalde

Kimika Fakultatea, Euskal Herriko Unibertsitatea and Donostia International Physics Center (DIPC), P.K. 1072 Donostia, Euskadi, Spain

ABSTRACT: The thermal stability of first-row transition-metal-doped TM@Zn$_i$S$_i$ nanoclusters, in which TM stands for the first-row transition metals from Sc to Zn and i = 12, 16, has been analyzed for the two lowest-lying spin states of each metal. These structures were previously characterized by Matxain et al. (Chem.—Eur. J. 2008, 14, 8547). We have seen that the metal atom can move toward the surface of the nanocluster, forming the so-called surface-doped structure. Hence, we have calculated the relative energies between these two isomers. Additionally, we have also characterized the transition states connecting both isomers and the energy barriers needed to move from one to another in order to predict the thermal stability of the endohedral compounds. These values are further used to predict the lifetimes of the endohedrally doped nanoclusters. Most of the lifetimes are predicted to be very small, although most of them are large enough for experimental detection. Conversely, the lifetimes of Zn@Zn$_{12}$S$_{12}$ and Zn@Zn$_{16}$S$_{16}$ have proved to be very large.

1. INTRODUCTION

Interest in nanoclusters made of II-VI compound semiconductors has grown spectacularly in recent years for their paramount technological potential owing to their special semiconductor properties that make these compounds suitable for applications such as photovoltaic solar cells, optical sensitizers, photocatalysts, quantum devices, or nanobiomedicine. [2] Moreover, nanoclusters made of these materials can be doped in order to modify their properties at will. In this context, spherical hollow nanoclusters provide the chance for endohedral doping, namely, the dopant is placed inside the cavity of the hollow nanoparticle. For instance, doping these nanoclusters endohedrally with transition metals leads to nanoclusters that would combine the appropriate optical and magnetic properties as to be used in nanomedicine, not only for improving of diagnosis applications but also in the development of tailored nanomaterials with therapeutic properties to treat, for example, the hyperthermic tumoral regression. [3]

In this work, we focus on first-row transition-metal-doped $TM@Zn_iS_i$ nanoclusters, where TM stands for the first-row transition metals (ScZn) and i = 12, 16. Of particular relevance to the present research is the previous characterization of the endohedral first-row transition-metal-doped $TM@Zn_iS_i$ nanoclusters, in which TM stands for the first-row transition metals from Sc to Zn and i = 12 and 16. [1] $Zn_{12}S_{12}$ and $Zn_{16}S_{16}$ were chosen because of their high stability, on account of their high symmetry and highly spheroidal shape, that allows for favored endohedral structures as compared to other nanoclusters. [4] In this previous work by Matxain et al., [1] they observed that the encapsulation free energies are negative, suggesting that these compounds are thermodynamically stable. They also undertook quantum molecular dynamics calculations for two selected cases, $Zn(1S)@Zn_{12}S_{12}$ and $Ti(5S)@Zn_{12}S_{12}$, as representative of the endohedral nanoclusters with the trapped atom at the center and off-center, respectively. These calculations confirmed the thermal stability of these two compounds. In addition, it was observed that there is negligible charge transfer between the dopant transition metals and their hollow cluster hosts and that, after encapsulaption, the spin densities remain localized on the transition-metal atoms. This points to an atomic-like behavior of the trapped transition-metal atom, which gives rise to atomic-like magnetic properties in a protected environment. Consequently, endohedral transition-metal compounds are interesting also due to their magnetic properties, which should yield dimers with (anti)ferromagnetic coupling. [5]

In this work we have further studied the thermal stability of these previously characterized endohedral clusters, [1] by carrying out quantum molecular dynamics calculations for several $TM@Zn_iS_i$ (i = 12, 16). It has been observed that some of these endohedrally doped nanoclusters are not thermally stable, for the dopant atom moves from the inner part of the cluster to the surface. These latter structures will be called surface-doped structures hereafter. In order to complement the quantum molecular dynamics simulations, we have additionally characterized the surface-doped structures for all compounds, along with the transition states connecting both isomers. In this manner we have estimated the lifetime of each endohedral

nanocluster using the calculated energy barriers for the endohedral-doped to surface-doped transformations.

Nevertheless, we would like to emphasize that both techniques are approximate. On the one hand, one single MD simulation is not representative, i.e., we are replacing a full sampling on the appropriate statistical ensemble by a single trajectory. On the other, the Eyring model is an approximation per se to calculate lifetimes and reaction rate constants. In addition, these lifetimes are calculated from the reaction rate constants. These reaction rate constants are very sensitive with respect to the activation energies. Consequently, the data obtained with both methodologies should not be taken quantitatively, but qualitatively.

2. METHODS

All geometries have been fully optimized using the gradient-corrected hybrid B3LYP 68 functional within the KohnSham implementation 9 of density functional theory. 10 Harmonic vibrational frequencies are determined by analytical differentiation of gradients, in order to determine whether the structures found are true minima or transition states and to extract zero-point energies and enthalpy and entropy contributions to Gibbs free energy, G, which is reported at room temperature. The relativistic compact effective core potentials and shared-exponent basis set 11 of Stevens et al. (SKBJ) have been used for Zn and S, as described in the study of the isolated clusters, 12 and also for the Zn atom when it acts as the dopant atom in order to be consistent with the structure. On the other hand, the fully relativistic multielectron fit pseudopotentials, with 10 electrons in the core, developed by Dolg et al., were used for the trapped atoms from Sc to Cu. 13,14 Nevertheless, we have done a few calculations to check the reliability of this method using a different basis set for Zn and for the rest of the transition metals.

$Zn@Zn_iS_i$ endohedral and surface-doped structures with both SKBJ and the Stuttgart basis set were optimized, and there is not any significant change since the relative stability between both isomers stays constant [$Zn@Zn_{12}S_{12}$ (SKBJ), ΔG surfend = 4.73 kcal/mol; $Zn@Zn_{12}S_{12}$ (Stuttgart), ΔG surfend = 2.51 kcal/mol; $Zn@Zn_{16}S_{16}$ (SKBJ), ΔG surfend = 1.45 kcal/mol; $Zn@Zn_{16}S_{16}$ (Stuttgart), ΔG surfend = 3.55 kcal/mol]. The same conclusion was reached from the calculations of $Cu@Zn_iS_i$ [$Cu@Zn_{12}S_{12}$ (SKBJ), ΔG surfend = 9.91 kcal/mol; Cu@ $Zn_{12}S_{12}$ (Stuttgart), ΔG surfend = 9.97 kcal/mol; $Cu@Zn_{16}S_{16}$ - (SKBJ), ΔG surfend = 7.96 kcal/mol; $Cu@Zn_{16}S_{16}$ (Stuttgart), ΔG surfend = 8.10 kcal/mol).

Note that pure angular momentum functions were used throughout this study. All the geometry optimizations and frequency calculations were carried out with the Gaussian 03 package. 15 The transition states between the characterized endohedral nanoclusters and their corresponding surface-doped structures have been calculated using the STQN method for locating transition structures. 16,17 Intrinsic reaction coordinate (IRC) calculations 18,19 [GS89, GS190] are further performed to assess that the calculated transition states connect the

appropriate reactants and products. All the atomic charges are calculated from the trace of the atomic polar tensor.

To further explore the thermal stability of these compounds, we undertook ab-initio thermal MD simulations at 298 K on some selected cases, controlled by means of the Nose thermostat as implemented in the SIESTA code, 20 within the DFT approach. Exchange and correlation effects were described using the generalized gradient approximation (GGA), within the revised Perdew BurkeErnzerhof (rPBE) functional. 2123 Core electrons were replaced by TroullierMartins norm-conserving pseudopotentials 24 in the Kleinman Bylander factored form. 25 Within the context of SIESTA, the use of pseudopotentials imposes basis orbitals adapted to them. Furthermore, SIESTA employs a localized basis set to represent the KohnSham orbitals for valence electrons. Accordingly, the basis set of atomic orbitals is constructed from numerical solutions of the atomic pseudopotential and are constrained to be zero beyond a cutoff radius. We used one basis set of double-z plus polarization quality (DZP). The single parameter (orbital energy shift) that defines the confinement radii of different orbitals was ΔE PAO = 150 meV, which gives typical precision within the accuracy of the used GGA functional. With this basis set, SIESTA calculates the self-consistent potential on a grid in real space. The fineness of this grid is determined in terms of an energy cutoff in analogy to the energy cutoff when the basis set involves plane waves. In our calculations, we used an equivalent plane wave cutoff energy of 200 Ry. These simulations were carried out for 5 ps with a chosen time step of 1 fs.

3. RESULTS

First of all, in subsection 3.1 we present the results for the ab-initio molecular dynamics simulations on two selected cases, namely, $Mn(4D)@Zn_{12}S_{12}$ and $Ni(1D)@Zn_{16}S_{16}$. Then, in subsections 3.2 and 3.3 the surface-doped and TS structures are characterized.

3.1. Quantum Molecular Dynamics. In ref 1, Matxain et al. carried out quantum molecular dynamics for two selected cases, $Zn(1S)@Zn_{12}S_{12}$ and $Ti(5S)@Zn_{12}S_{12}$. These calculations confirmed the thermal stability of these two compounds, since in both cases the dopant atom was kept inside the cage. We have extended these calculations for the remaining transition metals and here we present two selected cases, $Mn(4D)@Zn_{12}S_{12}$ and $Ni(1D)@Zn_{16}S_{16}$, where the guest transition metal does not remain confined in the cavity but moves to the surface of the nanocluster. We have set a simulation time of 5 ps, with a time step of 1 fs, and the trajectories have been calculated at a constant average temperature of 298 K.

Figure 1 shows how the energies vary during the simulation. It can be observed in both cases that, at a given time, the energy decreases noticeably. This happens when the transition metal moves toward the surface of the nanocluster, which leads to a more stable structure. Together with the total energy pictures, the representations of the distance of the Mn and Ni, respectively, from the center of mass of the nanoclusters during the simulation time, confirm that the guest atom moves away from the center. Likewise, the final structures of these two clusters are depicted. Observe that in the resulting structures the Mn and the Ni that were initially at the center of the cage lies on the surface of their corresponding clusters interacting covalently with

the Zn and S atoms adjacent to them. Therefore, quantum dynamics calculations of these selected cases suggest that they are not thermally stable and the TM would move toward the surface of the cage through a transition state. In the next subsections we will discuss the characterization of these surface-doped and transition state structures, in order to rationalize the behavior and stability of these compounds.

3.2. Surface Structures. In this subsection the nanoclusters with the corresponding transition metal at the surface will be analyzed and their properties will be discussed. For each TM, the two lowest-lying spin states have been considered, like in the endohedrally doped ones. 1 In Table 1 the geometrical, electronic, and energetic properties of the characterized local minima are given. The spin densities of each metal and the maximum spin density of zinc and sulfur atoms in the surface-doped and endohedral compounds are shown in Table 2. The spin densities of the transition metals in the endohedral nanoclusters are taken from the work of Matxain and co-workers. 1 Hereinafter, a comparison between endohedral nanoclusters and surface-doped structures will be made.

The surface-doped compounds do not resemble the square-hexagon structure of bare spheroids in the neighborhood of the TM. The TM breaks some of the ZnS bonds and forms new polarized covalent bonds with a number of Zn and S atoms. Depending on the TM, the number of bonds, i.e., the coordination number changes, as can be seen in Table 1. To determine the coordination number, we have considered a bond when the bond length between two atoms is smaller than the sum of their van der Waals radii. Different local minima have been characterized for each TM, from two-coordinated to six-coordinated structures. For the sake of clarity, the properties presented here are those corresponding to the most stable isomer of the surface-doped structure. For further information about other isomers, see the Supporting Information.

For Ti(5F), Mn(4D), Co(2F), Co(4F), and Zn(1S), the coordination number is the same in both Zn 12 S 12 and Zn 16 S 16 compounds. There are mainly two facts that must be pointed out regarding the coordination number of the metals in these surface-doped structures.

On one hand, in most of the nanoclusters, the coordination number is higher or the same in $TMZn_{12}S_{12}$ compared to $TMZn_{16}S_{16}$ compounds. On the other hand, in most cases low-spin compounds are higher coordinated than high-spin ones. Combining these two facts, we observe that the highest coordinated compound is $Ni(1S)Zn_{12}S_{12}$. There are a few exceptions. For instance, the high-spin compounds are higher-coordinated than the low-spin ones for $VZn_{12}S_{12}$, $ScZn_{16}S_i$ and $TiZn_{16}S_{16}$.

Looking at the energy difference between the surface-doped and endohedral nanoclusters, ΔG surfend , which is defined as G surf G end , it is clear that the surface-doped compounds are thermodynamically more stable than the corresponding endohedral ones, except for Zn(1 S)@$Zn_{16}S_{16}$ and Cr-(7S)@$Zn_{16}S_{16}$ (the latter one is remarkable for its large spin momentum). However, kinetically the endohedral compounds could be metastable. Large enough barriers

would prevent the TM from moving toward the surface. The kinetics of these reactions will be analyzed in subsection 3.3.

The relative energies between the high-spin and low-spin state of each compound are shown in Table 1. These values reveal that transition-metal surface-doped structures favor the low-spin states, with the exception of the middle transition metals, unlike the endohedral nanoclusters, where high-spin were, in general, more stable than the low-spin compounds. In general, the charges of the transition metals, given in Table 1, are larger in the surface-doped structures than in the endohedral ones. In the endohedral cases, most of the atomic charges reported by Matxain and co-workers 1 were lower than 0.2. Therefore, the TM trapped inside maintains its atomic-like properties, the interaction with the cage being weak. In surface-doped structures, on the other hand, the TM now interacts strongly with the cage, in fact, it is part of the cage and is covalently bonded to other atoms. Therefore, the charge of the TM is larger in this case. The spin densities given in Table 2 also support this idea: comparing the spin densities of the charactized structures and the values corresponding to their multiplicities, in most cases, they are more similar in the endohedral compounds than in surface nanoclusters. So, the interaction between the guest and the host is bigger in the latter.

3.3. Transition States. The endohedral and surface-doped structures are connected by a transition state (TS), a maximum in a reaction coordinate, as was observed in the quantum dynamics simulations. In this subsection, we have characterized these transition states in order to analyze the kinetic and thermal stability of the endohedral compounds. Although surface-doped structures are thermodynamically more stable, large enough barriers would prevent endohedral compounds from rearrange into the surface-doped structures. In Table 3 the energy barriers between the endohedral structures and the TS, $\Delta G^{\ddagger}$, the reaction rate constants (k), and the lifetimes of the endohedral compounds are given. The calculated energy barriers, $\Delta G^{\ddagger}$, are calculated as $\Delta G^{\ddagger} = \Delta G_{TS} - \Delta G_{end}$. These values are further used to calculate the reaction rate constants (k), at room temperature, using the Eyring equation

$$k = \frac{k_{\mathrm{B}} T}{h} e^{-\Delta G^{\ddagger}/RT}$$

where k is the reaction rate constant, T is the absolute temperature, $\Delta G^{\ddagger}$ is the energy barrier as defined above, k_{B} is the Boltzmann constant, h is the Planck's constant, and R is the gas constant. The lifetime of each endohedral nanocluster is then calculated as the inverse of the reaction rate constant. It is important to note that the reaction rate constants calculated are approximate, because the Eyring model has been used as well as because they are very sensitive with respect to the calculated activation energies, there being an exponential dependence between them. So, our aim is to have qualitative information about the stability of the endohedral nanoclusters and to point out potential stable structures.

At first glance, it is worth noticing that most of the calculated lifetimes are very small, although most of them are predicted to be large enough for experimental detection. We must emphasize that the lifetimes of $Zn(1S)@Zn_{12}S_{12}$ and $Zn(1S)@Zn_{16}S_{16}$ are the largest ones, being 2.86 days and 836 years, respectively. To explain this fact, we have to take into account that, in the endohedral compounds, the interaction between the guest and the host is very weak, while in the surface-doped structures this interaction is stronger. Moreover, the 3d-orbital shell in the Zn atom is full. Hence, Zn is the least reactive of all the first-row transition metals. This fact also explains why the endohedral $Zn(1S)@Zn_{16}S_{16}$ is thermodynamically more stable than the surface-doped $Zn(1S)Zn_{16}S_{16}$. Additionally, lifetimes reveal that endohedral nanoclusters favor high-spin states which coincide with the most stable endohedrally doped nanoclusters.

In subsection 3.1 we described the results of the quantum dynamics simulations of $Mn(4D)@Zn_{12}S_{12}$ and $Ni(1S)@Zn_{16}S_{16}$ and observed that after a few picoseconds the endohedral compounds converted into the more stable surface-doped structures. Notice that the calculated energy barriers for these compounds are 3.93 and 2.13 kcal/mol, respectively. These small barriers explain the obtained dynamical results. In the same vein, the energy barriers calculated for $Zn(1S)@Zn_{12}S_{12}$ and $Zn(1S)@Zn_{16}S_{16}$ are the largest ones. The dynamical behavior of the former was analyzed in the previous work by Matxain et al. [1] They carried out a quantum molecular dynamic simulation of 5 ps and they observed that in the endohedral structure the Zn atom remained confined at the center of the nanocluster, in agreement with the large energy barrier.

We have performed a longer simulation of 30 ps for this compound, to further confirm its thermal stability. In Figure 2 it is observed that the energy oscillates around the same value during all the simulation time and that the Zn atom moves around the center of the nanocluster along the simulation up to a maximum radial distance of 0.55 Å. The average radial separation of the caged Zn atom is 0.27 +- 0.11 Å. In addition, the trajectory of the zinc atom along the simulation time is also depicted in Figure 2. Therefore, this nanocluster is predicted to be thermally stable enough to survive a long time at room temperature to allow for its experimental detection.

4. CONCLUSIONS

The thermal stability of the first-row transition-metal-doped $TM@Zn_iS_i$ nanoclusters, in which TM stands for the first-row transition metals from Sc to Zn and i = 12, 16, has been analyzed by using two different methodologies. The first one is to carry out quantum molecular dynamic simulations, in which atoms and molecules are allowed to interact for a period of time, giving a view of the motion of the particles. This technique allows us to predict the thermal stability of $Zn(1S)@Zn_{12}S_{12}$, while $Mn(4D)@Zn_{12}S_{12}$ and $Ni(1S)@Zn_{16}S_{16}$ are seen to be thermally unstable. In these cases, the TM moves toward the surface, leading to the more stable surface-doped structures. The large number of $TM@Zn_iS_i$ structures along with the high cost of each quantum dynamical simulation made it impossible to carry out these simulations for all structures. Therefore, we have followed another methodology to study the thermal stability of the endohedral compounds. On the basis of the calculated energy differences between the

endohedral compounds and the TS compounds that connect the former with the surface-doped structures, we have estimated the lifetime of each endohedral structure. As mentioned before, these techniques are approximate. Hence, the data obtained have not to be taken quantitatively, but qualitatively. Thus, our aim is to point out potential stable structures. In this vein, both methodologies are in agreement in predicting $Zn(1S)@Zn_{12}S_{12}$ and $Zn(1S)@Zn_{16}S_{16}$ as the most stable structure with a lifetime of around 3 days and 900 years, respectively. The other endohedral compounds have much smaller lifetimes, although large enough for experimental detection.

ASSOCIATED CONTENT

Supporting Information. In Table 1 different isomers of surface-doped $TMZn_{12}S_{12}$ are depicted and in Table 2 the local minima of $TMZn_{16}S_{16}$ along with their corresponding energies are given. This material is available free of charge via the Internet at http://pubs.acs.org.

Corresponding Author

*E-mail: elisa.jimenez@ehu.es.

REFERENCES

(1) Matxain, J. M.; Formoso, E.; Mercero, J. M.; Piris, M.; Lopez, X.; Ugalde, J. M. Magnetic endohedral transition-metal-doped semiconducting-nanoclusters. Chem.—Eur. J. 2008, 14, 8547.

(2) Stroscio, M. A.; Dutta, M. editors. Kluwer, New York, 2004. (3) Dennis, C. L.; Jackson, A. J.; Borchers, J. A.; Hoopes, P. J.; Strawbridge, R.; Foreman, A. R.; Van Lierop, J.; Gruttner, C.; Ivkov, R. Nanotechnology 2009, 20, 395103.

(4) Hamad, S.; Catlow, C. R. A; Spano, E.; Matxain, J. M.; Ugalde, J. M. Structure and properties of ZnS nanoclusters. J. Phys. Chem. B 2005, 109, 2703.

(5) Matxain, J. M.; Piris, M.; Formoso, E.; Mercero, J. M.; Lopez, X.; Ugalde, J. M. Endohedral stannaspherenes: Mn@sn12 and its dimer: Ferromagnetic or antiferromagnetic? ChemPhysChem 2007, , 2096.

(6) Becke, A. D. Density-functional exchange-energy approximation with correct asymptotic behavior. Phys. Rev. A 1998, 38, 3098.

(7) Becke, A. D. A new mixing of HartreeFock and local density-functional theories. J. Chem. Phys. 1993, 98, 1372.

(8) Lee, C.; Yang, W.; Parr, R. G. Development of the ColleSalvetti correlation-energy formula into a functional of the electron density. Phys. Rev. B 1988, 37, 785.

(9) Kohn, W.; Sham, L. J. Self-consistent equations including exchange and correlation effects. Phys. Rev. 1965, 140, A1133.

(10) Hohenberg, P.; Kohn, W. Inhomogeneous electron gas. Phys. Rev. 1964, 136, B864.

(11) Stevens, W. J.; Krauss, M.; Basch, H.; Jasien, P. G. Relativistic compact effective potentials and efficient, shared exponent basis sets for the third, fourth and fifth row atoms. Can. J. Chem. 1992, 70, 612.

(12) Matxain, J. M.; Fowler, J. E.; Ugalde, J. M. Small clusters of IIVI materials: $Zn_i O_i$, i = 19. Phys. Rev. A 2000, 61, 53201.

(13) Dolg, M.; Wedig, U.; Stoll, H.; Preuss, H. Energy-adjusted ab initio pseudopotentials for the first row transition elements. J. Chem. Phys. 1987, 86, 866.

(14) Martin, J. M. L.; Sundermann, A. Correlation consistent valence basis sets for use with the StuttgartDresdenBonn relativistic effective core potentials: The atoms GaKr and InXe. J. Chem. Phys. 2001, 114, 3408.

(15) Frisch, M. J.; Trucks, G. W.; Schlegel, H. B.; Scuseria, G. E.; Robb, M. A.; Cheeseman, J. R.; Montgomery, J. A.; Vreven, T.; Kudin, K. N.; Burant, j: C.; Millam, J. M.; Iyengar, S. S.; Tomasi, J.; Barone, V.; Mennucci, B.; Cossi, M.; Scalmani, G.; Rega, N.; Petersson, G. A.; Nakatsuji, H.; Hada, M.; Ehara, M.; Toyota, K.; Fukuda, R.; Hasegawa, J.; Ishida, M.; Nakajima, T.; Honda, Y.; Kitao, O.; Nakai, H.; Klene, M.; Li, X.; Knox, J. E.; Hratchian, H. P.; Cross, J. B.; Bakken, V.; Adamo, C.; Jaramillo, J.; Gomperts, R.; Stratmann, R. E.; Yazyev, O.; Austin, A. J.; Cammi, R.; Pomelli, C.; Ochterski, J. W.; Ayala, P. Y.; Morokuma, K.; Voth, G. A.; Salvador, P.; Dannenberg, J. J.; Zakrzewski, V. G.; Dapprich, S.; Daniels, A. D.; Strain, M. C.; Farkas, O.; Malick, D. K.; Rabuck, A. D.; Raghavachari, K.; Foresman, J. B; Ortiz, J. V.; Cui, Q.; Baboul, A. G.; Clifford, S.; Cioslowski, J.; Stefanov, B. B.; Liu, G.; Liashenko, A.; Piskorz, P.; Komaromi, I.; Martin, R. L.; Fox, D. J.; Keith, T.; Al-Laham, M. A.; Peng, C. Y.; Nanayakkara, A.; Challacombe, M.; Gill, P. M. W.; Johnson, B.; Chen, W.; Wong, M. W.; Gonzalez, C.;Pople, J. A. Gaussian 03, Revision C.02; Gaussian, Inc., Wallingford, CT, 2004.

(16) Peng, C.; Schlegel, H. B. Isr. J. Chem. 1993, 33, 449.

(17) Peng, C.; Ayala, P. Y.; Schlegel, H. B.; Frisch, M. J. Using redundant internal coordinates to optimize equilibrium geometries and transition states. J. Comput. Chem. 1996, 17, 49.

(18) Gonzalez, C.; Schlegel, H. B. An improved algorithm for reaction path following. J. Chem. Phys. 1989, 90, 2154.

(19) Gonzalez, C.; Schlegel, H. B. Reaction path following in mass-weighted internal coordinates. J. Phys. Chem. 1990, 94, 5523.

(20) Soler, J. M.; Artacho, E.; Gale, J. D.; Garcia, A.; Junquera, J.; Ordejon, P.; Sanchez-Portal, D. J. Phys.: Condens. Matter 2002, 14, 2745.

(21) Perdew, J. P.; Burke, K.; Ernzerhof, M. Generalized gradient approximation made simple. Phys. Rev. Lett. 1996, 77, 3865.

(22) Zhang, Y.; Yang, W. Comment on generalized gradient approximation made simple?. Phys. Rev. Lett. 1998, 80, 890.

(23) Hammer, B.; Hansen, B. L.; Norskov, J. K. Improved adsorption energetics within density-functional theory using revised Perdew BurkeErnzerhof functionals. Phys. Rev. B 1999, 59, 7413.

(24) Troullier, N.; Martins, J. L. Efficient pseudopotentials for plane-wave calculations. Phys. Rev. B 1991, 43, 1993.

(25) Kleinman, L.; Bylander, D. M. Efficacious form for model pseudopotentials. Phys. Rev. Lett. 1982, 48, 1425.
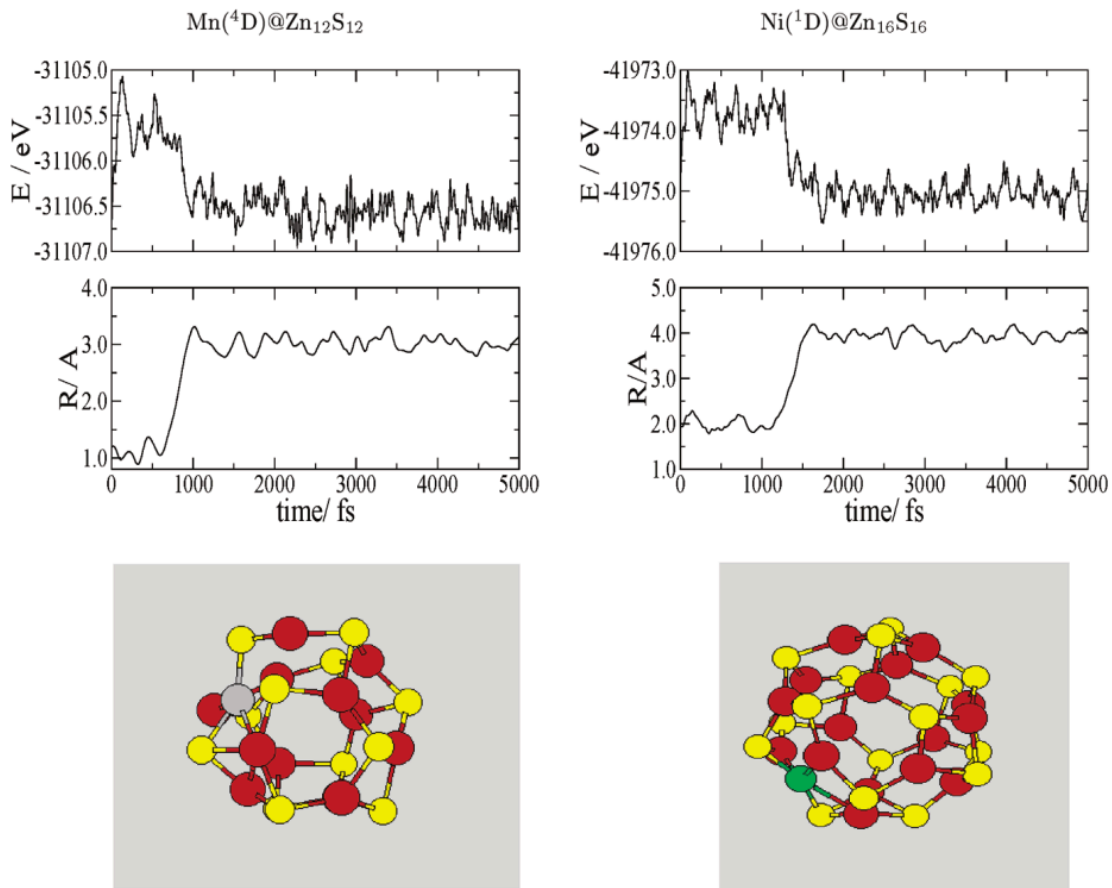
Figure 1. (Top) The variation of the energy, in eV, and the distance of the TM from the center of mass of the nanocluster, in Å, as a function of time, in fs. (Bottom) The resulting structures for Mn(4 D)@Zn 12 S 12 and Ni(1 D)@Zn 16 S 16 , respectively. S atoms are drawn in yellow, Zn atoms are drawn in red, and Mn is drawn in gray, while Ni is drawn in green.

		TM$-$Zn$_{12}$S$_{12}$				TM$-$Zn$_{16}$S$_{16}$			
TM	2S+1	q_x	CN	ΔE	$\Delta G_{surf-end}$	q_x	CN	ΔE	$\Delta G_{surf-end}$
Sc	2	0.69	5	0.00	–	0.70	3	0.00	-50.23
Sc	**4**	0.60	3	2.16	–	0.58	4	9.86	–
Ti	3	0.29	5	0.00	–	0.39	3	0.00	-40.77
Ti	**5**	0.28	4	18.32	-17.42	0.51	4	21.51	-10.45
V	**4**	0.43	2	0.00	-26.22	0.71	3	0.00	-52.35
V	**6**	0.05	5	5.10	-13.88	0.26	2	25.39	-6.36
Cr	**5**	0.16	4	0.00	-29.65	0.39	3	0.00	-27.84
Cr	7	0.29	4	12.54	-2.29	0.33	2	12.78	0.73
Mn	**4**	0.61	4	13.22	-33.81	0.43	4	15.43	-30.29
Mn	6	0.36	2	0.00	-22.62	0.77	3	0.00	-15.67
Fe	**3**	0.21	4	5.39	-20.60	0.20	3	14.37	-14.82
Fe	5	0.25	2	0.00	-19.55	0.57	3	0.00	-22.44
Co	**2**	0.15	4	0.00	-21.52	0.11	4	5.66	-11.53
Co	4	0.21	2	0.99	-11.98	0.25	2	0.00	-21.04
Ni	**1**	-0.22	6	0.00	–	-0.26	5	0.00	-20.00
Ni	3	0.23	5	7.31	-15.58	0.32	4	5.25	-14.31
Cu	2	0.23	5	–	-9.97	0.16	2	–	-8.10
Zn	1	0.29	2	–	-4.73	0.32	2	–	1.45

Table 1. Charge of Transition-Metal Atom and the Coordination Number [a]
[a] ΔE is the relative energy between the low-spin state and the high-spin state, and $\Delta G_{end-surf}$ is the energy difference between the endohedral and the surface-doped structures, both in kcal/mol. The ground spin-state of each metal is in bold.

		$\rho_{S_{TM}}$			
		Zn$_{12}$S$_{12}$		Zn$_{16}$S$_{16}$	
TM	2S+1	surface structures	endohedral structures	surface structures	endohedral structures
Sc	2	0.74	–	0.99	0.87
Sc	4	1.45	–	1.26	–
Ti	3	2.00	–	2.06	1.86
Ti	5	3.00	3.17	2.89	3.49
V	4	3.27	2.91	3.18	2.86
V	6	4.15	4.46	4.42	4.61
Cr	5	4.45	3.94	4.35	3.94
Cr	7	5.11	5.53	5.37	5.61
Mn	4	4.27	3.16	4.14	3.35
Mn	6	5.04	4.65	4.86	4.80
Fe	3	2.84	2.23	2.52	2.27
Fe	5	3.82	3.60	3.65	3.85
Co	2	1.66	1.25	1.69	2.69
Co	4	2.69	2.70	2.69	2.90
Ni	3	1.36	1.64	1.47	1.71
Cu	2	0.22	0.66	0.41	0.70

Table 2. Spin Densities of the Transition Metals in Both Endohedral (TM@Zn$_{12}$S$_{12}$ and TM@Zn$_{16}$S$_{16}$) and Surface-Doped (TMZn$_{12}$S$_{12}$ and TMZn$_{16}$S$_{16}$) Compounds

		TM@Zn$_{12}$S$_{12}$				TM@Zn$_{16}$S$_{16}$			
TM	2S+1	freq	ΔG_{TS-end}	$K\,(s^{-1})$	$\tau\,(s)$	freq	ΔG_{TS-end}	$K\,(s^{-1})$	$\tau\,(s)$
Sc	2	–	–	–	–	–	–	–	–
Sc	4	–	–	–	–	–	–	–	–
Ti	3	–	–	–	–	–	–	–	–
Ti	5	71.9i	4.77	1.98×10^9	5.05×10^{-10}	–	–	–	–
V	4	42.6i	2.62	7.46×10^{10}	1.34×10^{-11}	–	–	–	–
V	6	74.4i	5.54	5.39×10^8	1.85×10^{-9}	63.2i	6.26	1.60×10^8	6.25×10^{-9}
Cr	5	62.3i	8.54	3.41×10^6	2.93×10^{-7}	68.1i	−19.8		
Cr	7	45.4i	12.45	4.64×10^3	2.15×10^{-4}	59.7i	14.95	6.83×10	1.46×10^{-2}
Mn	4	75.2i	3.93	8.17×10^9	1.22×10^{-10}	–	–	–	–
Mn	6	42.4i	11.95	1.08×10^4	9.26×10^{-5}	45.8i	15.11	5.21×10	1.92×10^{-2}
Fe	3	72.4i	4.87	1.67×10^9	5.98×10^{-10}	40.8i	1.36	6.25×10^{11}	1.60×10^{-12}
Fe	5	105.7i	6.73	7.24×10^7	1.38×10^{-8}	45.9i	2.93	4.42×10^{10}	2.26×10^{-11}
Co	2	75.2i	1.49	5.02×10^{11}	1.99×10^{-12}	54.9i	5.17	1.01×10^9	9.92×10^{-10}
Co	4	58.1i	10.12	2.37×10^5	4.22×10^{-6}	49.0i	5.29	8.23×10^8	1.22×10^{-9}
Ni	1	–	–			64.3i	2.13	1.71×10^{11}	5.86×10^{-12}
Ni	3	50.6i	0.80	1.61×10^{12}	6.21×10^{-13}	96.6i	12.18	7.32×10^3	1.36×10^{-4}
Cu	2	56.2i	6.50	1.07×10^8	9.37×10^{-9}	56.7i	5.02	1.30×10^9	7.70×10^{-10}
Zn	1	47.4i	24.81	4.04×10^{-6}	2.47×10^5	63.1i	31.66	3.85×10^{-11}	2.60×10^{10}

Table 3. Characterized Transition States between Endohedral Compounds and Their Respective Surface-Doped Compounds, for TM@Zn$_{12}$S$_{12}$ and TM@Zn$_{16}$S$_{16}$ [a]

[a] $\Delta G^{\ddagger}$ (kcal/mol) is the energy difference between the transition states and the endohedral structures, i.e., the activation energy. k is the calculated reaction rate constant (s^{-1}), and τ is the lifetime (s). The ground spin-state of each metal is in bold.
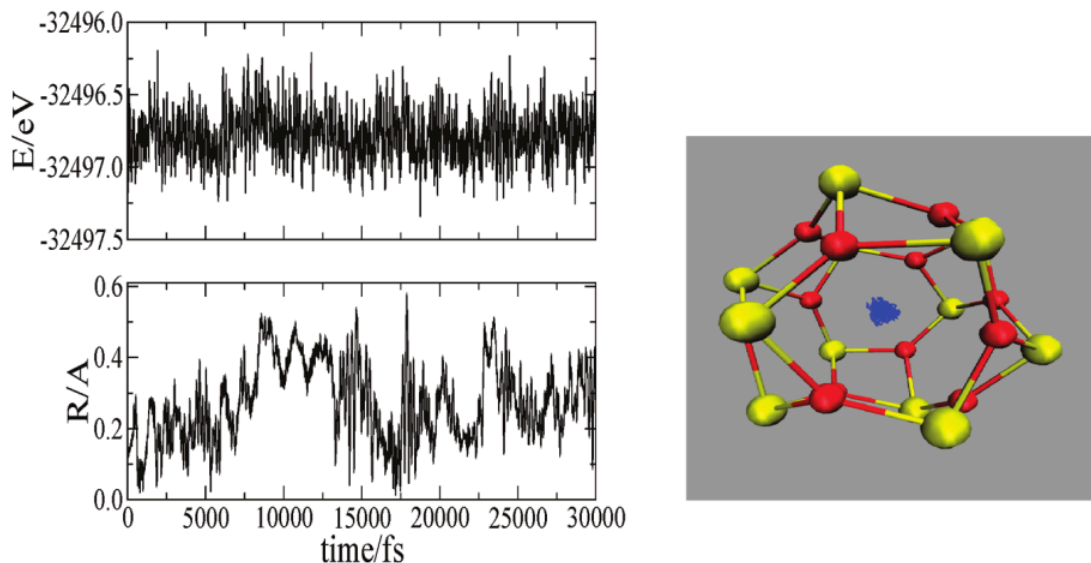
Figure 2. Quantum Dynamic simulation of Zn(1S)@Zn$_{12}$S$_{12}$. The variation of the energy (eV) and the variation of the distance R (Å) of the trapped atom from the center of mass of the nanocluster as a function of time during the simulation is depicted on the left. On the right, the movement of the trapped Zn atom inside the cage.